ADVERSARIAL ROBUSTNESS AS A PRIOR FOR LEARNED REPRESENTATIONS

Anonymous authors
Paper under double-blind review

ABSTRACT

An important goal in deep learning is to learn versatile, high-level *feature representations* of input data. However, standard networks' representations seem to possess shortcomings that, as we illustrate, prevent them from fully realizing this goal. In this work, we show that *robust optimization* can be re-cast as a tool for enforcing *priors* on the features learned by deep neural networks. It turns out that representations learned by robust models address the aforementioned shortcomings and make significant progress towards learning a high-level encoding of inputs. In particular, these representations are approximately invertible, while allowing for direct visualization and manipulation of salient input features. More broadly, our results indicate adversarial robustness as a promising avenue for improving learned representations.

1 INTRODUCTION

Beyond achieving remarkably high accuracy on a variety of tasks (Krizhevsky et al., 2012; He et al., 2015; Collobert & Weston, 2008), a major appeal of deep learning is the ability to learn effective *feature representations* of data. Specifically, deep neural networks can be thought of as linear classifiers acting on *learned feature representations* (also known as *feature embeddings*). A major goal in representation learning is for these embeddings to encode high-level, interpretable features of any given input (Goodfellow et al., 2016; Bengio et al., 2013; Bengio, 2019). Indeed, learned representations turn out to be quite versatile—in computer vision, for example, they are the driving force behind transfer learning Girshick et al. (2014); Donahue et al. (2014), and image similarity metrics such as VGG distance Dosovitskiy & Brox (2016a); Johnson et al. (2016); Zhang et al. (2018).

These successes and others clearly illustrate the utility of learned feature representations. Still, deep networks and their embeddings exhibit some shortcomings that are at odds with our idealized model of a linear classifier on top of interpretable high-level features. For example, the existence of adversarial examples (Szegedy et al., 2014)—and the fact that they may correspond to flipping predictive features Ilyas et al. (2019)—suggests that deep neural networks make predictions based on features that are vastly different from what humans use, or even recognize. (This message has been also corroborated by several recent works (Brendel & Bethge, 2019; Geirhos et al., 2019; Jetley et al., 2018; Zhang & Zhu, 2019).) In fact, we show a more direct example of such a shortcoming (c.f. Section 2), wherein one can construct pairs of images that appear completely different to a human but are nearly identical in terms of their learned feature representations.

Our contributions. Motivated by the limitations of standard representations, we propose using the robust optimization framework as a tool to enforce (user-specified) *priors* on features that models should learn (and thus on their learned feature representations). We demonstrate that the resulting learned "robust representations" (the embeddings learned by adversarially robust neural networks Goodfellow et al. (2015); Madry et al. (2018)) address many of the shortcomings affecting standard learned representations and thereby enable new modes of interaction with inputs via manipulation of salient features. These findings are summarized below (c.f. Figure 1 for an illustration):

- **Representation inversion (Section 4.1)**: In stark contrast to standard representations, robust representations are *approximately invertible*—that is, they provide a high-level embedding of the input such that images with similar robust representations are semantically

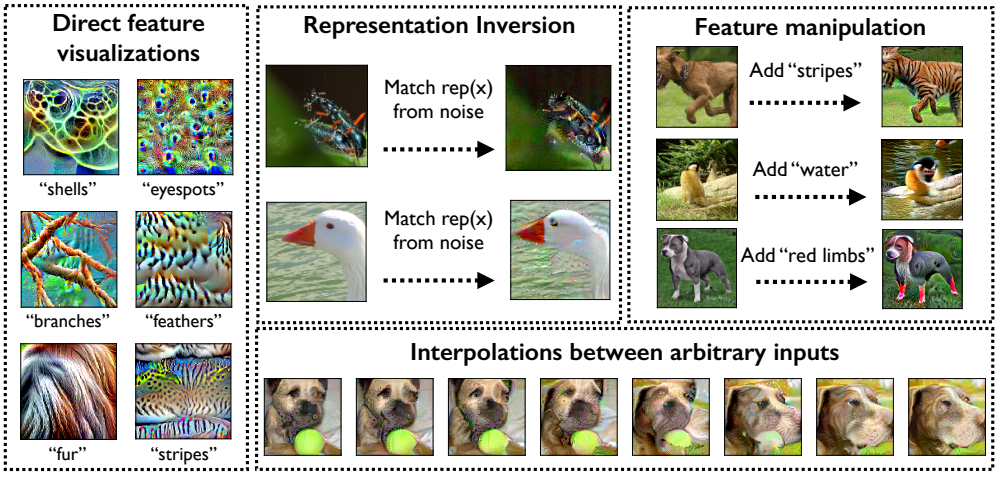

Figure 1: Sample images highlighting the properties and applications of "robust representations" studied in this work. All of these manipulations use only gradient descent on simple, unregularized, direct functions of the representations of adversarially robust neural networks Goodfellow et al. (2015); Madry et al. (2018).

similar, and the salient features of an image are easily recoverable from its robust feature representation. This property also naturally enables feature interpolation between arbitrary inputs.

- **Simple feature visualization (Section 4.2)**: Direct maximization of the coordinates of robust representations suffices to visualize easily recognizable features of the model. This is again a significant departure from standard models where (a) without explicit regularization at visualization time, feature visualization often produces unintelligible results; and (b) even with regularization, visualized features in the representation layer are scarcely human-recognizeable Olah et al. (2017).
- **Feature manipulation (Section 4.2.1)**: Through the aforementioned direct feature visualization property, robust representations enable the addition of specific features to images through direct first-order optimization.

Broadly, our results indicate that robust optimization is a promising avenue for learning representations that are more "aligned" with our notion of perception. Furthermore, our findings highlight the the desirability of adversarial robustness as a goal beyond the standard security and reliability context.

2 Limitations of standard representations

Following standard convention, for a given deep network we define the *representation* $R(x) \in \mathbb{R}^k$ of a given input $x \in \mathbb{R}^d$ as the activations of the penultimate layer of the network (where usually $k \ll d$). The prediction of the network can thus be viewed as the output of a linear classifier on the representation $R(x)$. We refer to the *distance in representation space* between two inputs (x_1, x_2) as the ℓ_2 distance between their representations $(R(x_1), R(x_2))$, i.e., $\|R(x_1) - R(x_2)\|_2$.

A common aspiration in representation learning is to have that for any pixel-space input x, $R(x)$ is a vector encoding a set of "human-meaningful" features of x Bengio (2019); Goodfellow et al. (2016); Bengio et al. (2013). These high-level features would be linearly separable with respect to the classification task, allowing the classifier to attain high accuracy.

Running somewhat counter to this intuition, however, we find that it is straightforward to construct pairs of images with nearly identical representations yet drastically different content, as shown in Figure 2. Finding such pairs turns out to be as simple as sampling two images $x_1, x_2 \sim \mathcal{D}$, then

optimizing one of them to minimize distance in representation space to the other:

$$x_1' = x_1 + \min_{\delta} \|R(x_1 + \delta) - R(x_2)\|_2. \tag{1}$$

Indeed, solving objective (1) yields images that have similar representations, but share no qualitative resemblance (in fact, x_1' tends to look nearly identical to x_1). We provide an example of such a pair (x_1', x_2) in Figure 2.

Note that if representations truly provided an encoding of any image into high-level features, finding images with similar representations should necessitate finding images with similar high-level features. Thus, the existence of these image pairs (and similar phenomena observed by prior work Jacobsen et al. (2019)) lays bare a misalignment between the notion of distance induced via the features learned by current deep networks, and the notion of distance as perceived by humans.

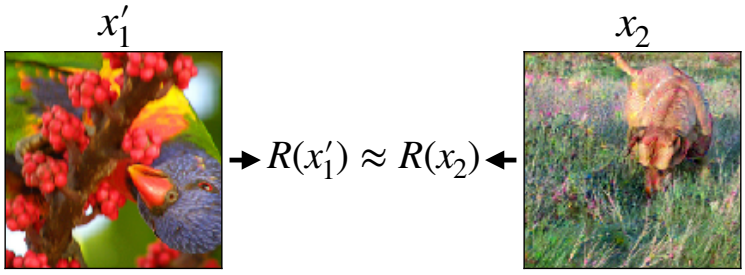

Figure 2: A limitation of standard neural network representations: it is straightforward to construct pairs of images (x_1', x_2) that appear completely different yet map to similar representations.

3 Adversarial robustness as a prior

Our analysis in Section 2 and prior work (Jacobsen et al., 2019) prompt the question:

How can we learn better-behaved representations?

In this work, we demonstrate that the representations learned by adversarially robust neural networks seem to address many identified limitations of standard representations, and make significant progress towards the broader goal of learning high-level, human-understandable encodings.

Adversarially robust deep networks and robust optimization. In standard settings, supervised machine learning models are trained by minimizing the expected loss with respect to a set of parameters θ, i.e., by solving an optimization problem of the form:

$$\theta^* = \min_{\theta} \mathbb{E}_{(x,y)\sim\mathcal{D}} \left[\mathcal{L}_\theta(x, y)\right]. \tag{2}$$

We refer to (2) as the *standard* training objective—finding the optimum of this objective should guarantee high performance on unseen data from the distribution. It turns out, however, that deep neural networks trained with this standard objective are extraordinarily vulnerable to *adversarial examples* (Szegedy et al., 2014)—by changing a natural input imperceptibly, one can easily manipulate the predictions of a deep network to be arbitrarily incorrect.

A natural approach (and one of the most successful) for defending against these adversarial examples is to use the *robust optimization framework*: a classical framework for optimization in the presence of uncertainty (Wald, 1945; Danskin, 1967). In particular, instead of just finding parameters which minimize the expected loss (as in the standard objective), a robust optimization objective also requires that the model induced by the parameters θ be robust to worst-case perturbation of the input:

$$\theta^* = \arg\min_{\theta} \mathbb{E}_{(x,y)\sim\mathcal{D}} \left[\max_{\delta\in\Delta} \mathcal{L}_\theta(x + \delta, y)\right]. \tag{3}$$

This robust objective is in fact common in the context of machine learning security, where Δ is usually chosen to be a simple convex set, e.g., an ℓ_p-ball. Canonical instantiations of robust optimization such as adversarial training (Goodfellow et al., 2015; Madry et al., 2018)) have arisen

as practical ways of obtaining networks that are invariant to small ℓ_p-bounded changes in the input while maintaining high accuracy (though a small tradeoff between robustness and accuracy has been noted by prior work Tsipras et al. (2019); Su et al. (2018)(also cf. Appendix Tables 4 and 5 for a comparison of accuracies of standard and robust classifiers)).

Robust optimization as a model prior. Traditionally, adversarial robustness in the deep learning setting has been explored as a goal predominantly in the context of ML security and reliability (Biggio & Roli, 2018).

In this work, we consider an alternative perspective on adversarial robustness—we cast it as a prior on the features that can be learned by a model. Specifically, models trained with objective (3) must be *invariant* to a set of perturbations Δ. Thus, selecting Δ to be a set of perturbations that humans are robust to (e.g., small ℓ_p perturbations) results in models that share more invariances with (and thus are encouraged to use similar features to) human perception. Note that incorporating human-selected priors and invariances in this fashion has a long history in the design of ML models—convolutional layers, for instance, were introduced as a means of introducing an invariance to translations of the input (Fukushima, 1980).

In what follows, we will explore the effect of the prior induced by adversarial robustness on models' learned representations, and demonstrate that representations learned by adversarially robust models are better behaved, and do in fact seem to use features that are more human-understandable.

4 Properties and applications of robust representations

In the previous section, we proposed using *robust optimization* as a way of enforcing user-specified priors during model training. Our goal was to mitigate the issues with standard representations identified in Section 2. We now demonstrate that the learned representations resulting from training with this prior indeed exhibit several advantages over standard representations.

Recall that we define a representation $R(\cdot)$ as a function induced by a neural network which mapping inputs $x \in \mathbb{R}^n$ to vectors $R(x) \in \mathbb{R}^k$ in the representation layer of that network (the penultimate layer). In what follows, we refer to "standard representations" as the representation functions induced by standard (non-robust) networks, trained with the objective (2)—analogously, "robust representations" refer to the representation functions induced by ℓ_2-adversarially robust networks, i.e. networks trained with the objective (3) with Δ being the ℓ_2 ball:

$$\theta^*_{robust} = \arg\min_\theta \mathbb{E}_{(x,y)\sim\mathcal{D}} \left[\max_{\|\delta\|_2 \leq \varepsilon} \mathcal{L}_\theta(x+\delta, y) \right].$$

It is worth noting that despite the value of ε used for training being quite small, we find that robust optimization *globally* affects the behavior of learned representations. As we demonstrate in this section, the benefits of robust representations extend to out-of-distribution inputs and far beyond ε-balls around the training distribution.

Experimental setup. We train robust and standard ResNet-50 networks on the Restricted ImageNet (Tsipras et al., 2019) and ImageNet (Russakovsky et al., 2015) datasets—training details are in Appendices A.2 and A.3, and the performance of each model is reported in Appendix A.4. In the main text, we present results for Restricted ImageNet, and link to (nearly identical) results for ImageNet present in the appendices (B.2.4,B.1.4).

Unless explicitly noted otherwise, our optimization method of choice for any objective function will be (projected) gradient descent (PGD), a first-order method which is known to be highly effective for minimizing neural network-based loss functions for both standard and adversarially robust neural networks (Athalye et al., 2018; Madry et al., 2018).

The code for reproducing our results is publicly available at `https://github.com/snappymanatee/robust-learned-representations`.

4.1 Inverting robust representations

As discussed in Section 2, for standard deep networks (2), given any input x, it is straightforward to find another input that looks entirely different but has nearly the same representation (c.f. Figure 2).

We noted that this finding runs somewhat counter to the idea that these learned representations effectively capture relevant input features. After all, if the representation function was truly extracting "high-level" features of the input as we conceptualize them, semantically dissimilar images should (by definition) have different representations. We now show that the state of affairs is greatly improved for robust representations.

Robust representations are (approximately) invertible out of the box. We begin by recalling the optimization objective (1) used in Section 2 to find pairs of images with similar representations, a simple minimization of ℓ_2 distance in representation space from a source image x_1 to a target image x_2:

$$x_1' = x_1 + \min_{\delta} \|R(x_1 + \delta) - R(x_2)\|_2. \tag{4}$$

This process can be seen as recovering an image that maps to the desired target representation, and hence is commonly referred to as *representation inversion* (Dosovitskiy & Brox, 2016b; Mahendran & Vedaldi, 2015; Ulyanov et al., 2017). It turns out that in sharp contrast to what we observe for standard models, the images resulting from minimizing (4) for robust models are actually *semantically similar* to the original (target) images whose representation is being matched, and this behavior is consistent across multiple samplings of the starting point (source image) x_1 (cf. Figure 3).

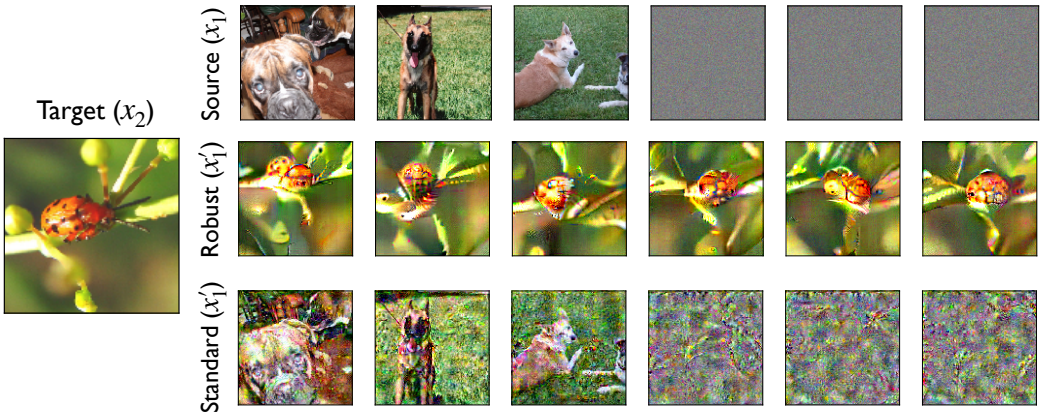

Figure 3: Visualization of inputs that are mapped to similar representations by models trained on the Restricted ImageNet dataset. *Target* (x_2) & *Source* (x_1): random examples image from the test set; *Robust* and *Standard* (x_1'): result of minimizing the objective (4) to match (in ℓ_2-distance) the representation of the target image starting from the corresponding source image for (*top*): a robust (adversarially trained) and (*bottom*): a standard model respectively. For the robust model, we observe that the resulting images are perceptually similar to the target image in terms of high-level features (even though they do not match it exactly), while for the standard model they often look more similar to the source image which is the seed for the optimization process. Additional results in Appendix B.2, and similar results for ImageNet are in Appendix B.2.4.

Representation proximity seems to entail semantic similarity. In fact, the contrast between the invertibility of standard and robust representations is even stronger. To illustrate this, we will attempt to match the representation of a target image while staying close to the starting image of the optimization in pixel-wise ℓ_2-norm (this is equivalent to putting a norm bound on δ in objective (4)). With standard models, we can consistently get close to the target image in representation space, without moving far from the source image x_1. On the other hand, for robust models, we cannot get close to the target representation while staying close to the source image—this is illustrated quantitatively in Figure 4. This indicates that for robust models, semantic similarity may in fact be necessary for representation similarity (and is not, for instance, merely an artifact of the local robustness induced by robust optimization).

We also find that even when δ is highly constrained (i.e. when we are forced to stay very close to the source image and thus cannot match the representation of the target well), the solution to the inversion problem still displays some salient features of the target image (c.f. Figure 5). Both of

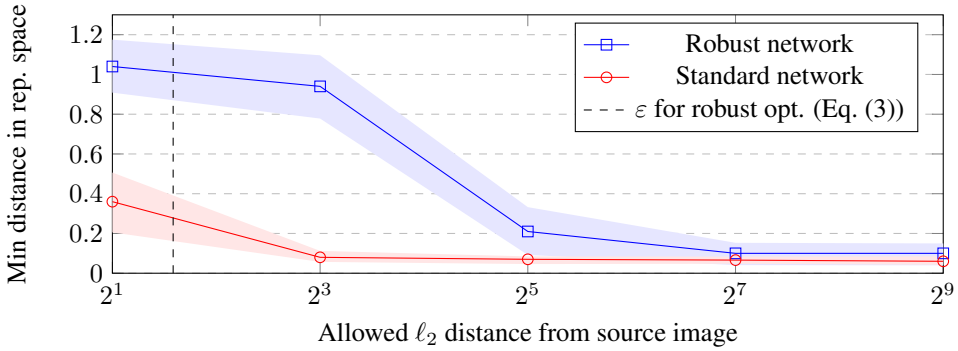

Figure 4: Optimizing objective (4) with PGD and an ℓ_2-norm constraint around the source image. On the x-axis is the radius of the constraint set, and on the y-axis is the distance in representation space between the minimizer of objective (4) within the constraint set and the target image, normalized by the norm of the representation of the target image: i.e., a point (x_i, y_i) on the graph corresponds to $y_i = \min_{\|\delta\|_2 \leq x_i} \|R(x+\delta) - R(x_{targ})\|_2 / \|R(x_{targ})\|_2$. Notably, we are unable to closely match the representation of the target image for the robust network until the norm constraint grows very large, and in particular much larger than the norm of the perturbation that the model is trained to be robust against (ε in objective (3)).

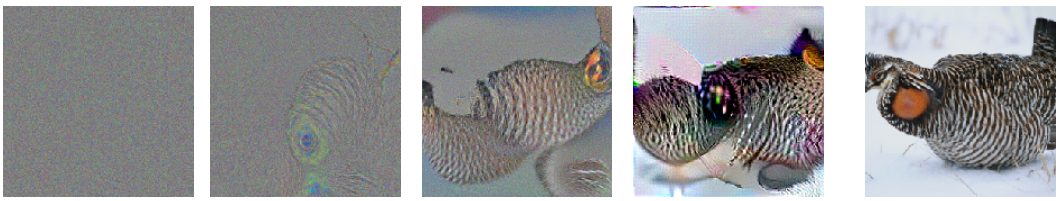

Figure 5: A visualization of the final solutions to the optimizing objective (4) with PGD when constraining the solution to lie in an ℓ_2 ball around the source image for an adversarially robust neural network. We note that even the radius of the constraint set is small and we cannot match the representation very well, salient features of the target image still arise.

these observations suggest that the representations of robust networks function much more like we would expect high-level feature representations to behave.

Inversion of out-of-distribution inputs. We find that the inversion properties uncovered above hold even for out-of-distribution inputs, demonstrating that robust representations capture *general* features as opposed to features only relevant for the specific classification task. In particular, we repeat the inversion experiment (simple minimization of distance in representation space) using images from classes not present in the original dataset used during training (Figure 6 right) and structured random patterns (Figure 18 in Appendix B.2): the reconstructed images consistently resemble the targets.

Interpolation between arbitrary inputs. Note that this ability to consistently invert representations into corresponding inputs also translates into the ability to *semantically interpolate* between any two inputs. For any two inputs x_1 and x_2, one can (linearly) interpolate between $R(x_1)$ and $R(x_2)$ in representation space, then use the inversion procedure to get images corresponding to the interpolate representations. The resulting inputs interpolate between the two endpoints in a perceptually plausible manner without any of the "ghosting" artifacts present in input-space interpolation. We show examples of this inversion as well as experimental details in Appendix A.5.

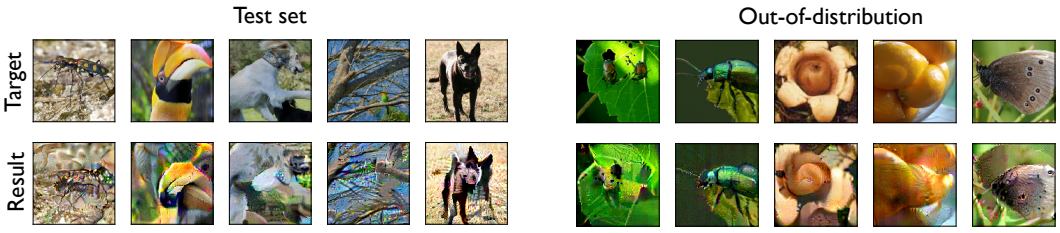

Figure 6: Robust representations yield semantically meaningful embeddings. *Target*: random images from the test set (col. 1-5) and from outside of the training distribution (6-10); *Result*: images obtained from optimizing inputs (using Gaussian noise as the source image) to minimize ℓ_2-distance to the representations of the corresponding image in the top row. (More examples appear in Appendix B.2.)

4.2 Direct feature visualization

A common technique for visualizing and understanding the representation function $R(\cdot)$ of a given network is *optimization-based feature visualization* (Olah et al., 2017), a process in which we maximize a specific feature (component) in the representation with respect to the input, in order to obtain insight into the role of the feature in classification. Concretely, given some $i \in [k]$ denoting a component of the representation vector, we use gradient descent to find an input x' that maximally activates it, i.e., we solve:

$$x' = \arg\max_{\delta} R(x_0 + \delta)_i \tag{5}$$

for various starting points x_0 which might be random images from $\mathcal{D}$ or even random noise.

Visualization "fails" for standard networks. For standard networks, optimizing the objective (5) often yields unsatisfying results. While we *can* easily find images for which the i^{th} component of $R(\cdot)$ is large (and thus the optimization problem is tractable), these images tends to look meaningless to humans, often resembling the starting point of the optimization. Even when these images are non-trivial, they tend to contain abstract, hard-to-discern patterns (c.f. Figure 7 (bottom)). As we discuss later in this section, regularization/post-processing of visualizations does improve this state of affairs, though not very significantly and potentially at the cost of suppressing useful features present in the representation post-hoc.

Robust representations allow for direct visualization of human-recognizable features. For robust representations, however, we find that easily recognizable high-level features emerge from optimizing objective (5) directly, *without any regularization or post-processing*. We present the results of this maximization in Figure 7 (top): coordinates consistently represent the same concepts across different choice of starting input x_0 (both in and out of distribution). Furthermore, these concepts are not merely an artifact of our visualization process, as they consistently appear in the test-set inputs that most strongly activate their corresponding coordinates (Figure 8).

The limitations of regularization for visualization in standard networks. Given that directly optimizing objective (5) does not produce human-meaningful images, prior work on visualization usually tries to regularize objective (5) through a variety of methods. These methods include applying random transformations during the optimization process (Mordvintsev et al., 2015; Olah et al., 2017), restricting the space of possible solutions (Nguyen et al., 2015; 2016; 2017), or post-processing of the input or gradients (Oygard, 2015; Tyka, 2016). While regularization does in general produce better results qualitatively, it comes with a few notable disadvantages that are well-recognized in the domain of feature visualization. First, when one introduces prior information about what makes images visually appealing into the optimization process, it becomes difficult to disentangle the effects of the actual model from the effect of the prior information introduced through regularization[1]. Furthermore, while adding regularization does improve the visual quality of the visualizations, the components of the representation still cannot be shown to correspond to

[1]In fact, model explanations that enforce priors for purposes of visual appeal have been often found to have little to do with the data or the model itself (Adebayo et al., 2018).

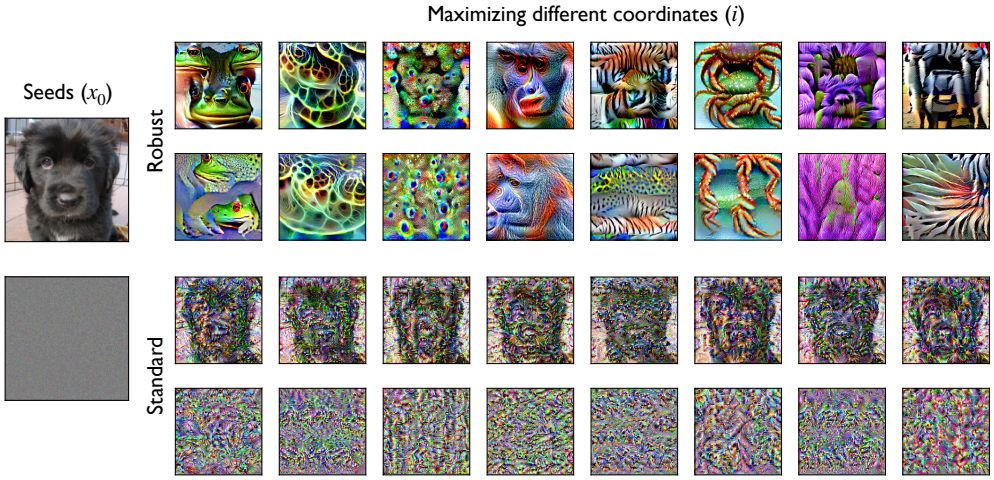

Figure 7: Correspondence between image-level patterns and activations learned by standard and robust models on the Restricted ImageNet dataset. Starting from randomly chosen seed inputs (noise/images), we use PGD to find inputs that (locally) maximally activate a given component of the representation vector (cf. Appendix A.6.1 for details). In the left column we have the seed inputs x_0 (selected *randomly*), and in subsequent columns we visualize the result of the optimization (5), i.e., x', for different activations, with each row starting from the same (far left) input x_0 for (*top*): a robust (adversarially trained) and (*bottom*): a standard model. Additional visualizations in Appendix B.1, and similar results for ImageNet in B.1.4.

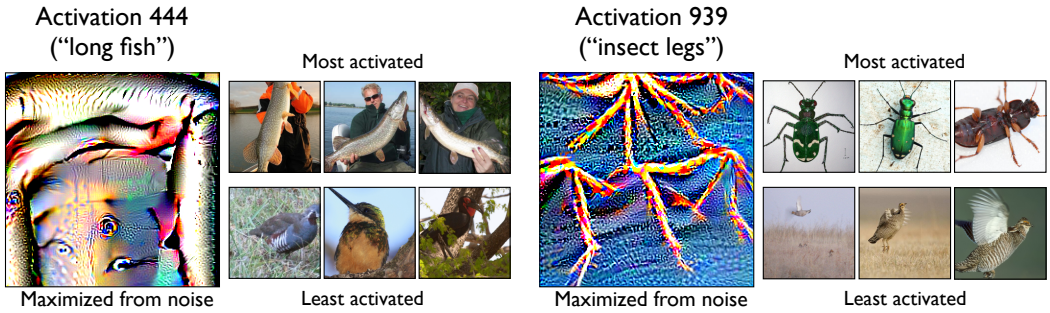

Figure 8: Maximizing inputs x' (found by solving (5) with x_0 being a gray image) and most activating images (from the test set) for two *random* activations of a robust model trained on the Restricted ImageNet dataset. In addition to finding maximizing inputs (as in the bottom row of Figure 7), we plot the top three and bottom three images (labeled "most activated" and "least activated" respectively) from the validation set, sorted by the magnitude of the selected activation.

any recognizable high-level feature. Indeed, Olah et al. (2017) note that in the representation layer of a standard GoogLeNet, "Neurons do not seem to correspond to particularly meaningful semantic ideas"—the corresponding feature visualizations are reproduced in Figure 9. We also provide examples of representation-layer visualizations for VGG16 (which we found qualitatively best among modern architectures) regularized with jittering and random rotations in Figure 10. While these visualizations certainly look better qualitatively than their unregularized counterparts in Figure 7 (bottom), there remains a significantly large gap in quality and discernability between these regularized visualizations and those of the robust network in Figure 7 (top).

4.2.1 Natural consequence: feature manipulation

The ability to directly visualize high-level, recognizable features reveals another application of robust representations, which we refer to as *feature manipulation*. Consider the visualization objective (5) shown in the previous section. Starting from some original image, optimizing this objective

Figure 9: Figure reproduced from (Olah et al., 2017)—a visualization of a few components of the representation layer of GoogLeNet. While regularization (as well as Fourier parameterization and colorspace decorrelation) yields visually appealing results, the visualization does not reveal consistent semantic concepts.

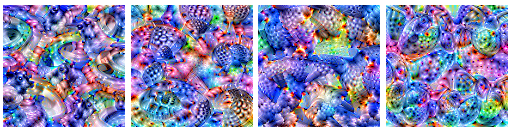

Figure 10: A visualization of the first four components of the representation layer of VGG16 when regularization via random jittering and regularization is applied. Figure produced using the Lucid[a] visualization library.

[a] https://github.com/tensorflow/lucid/

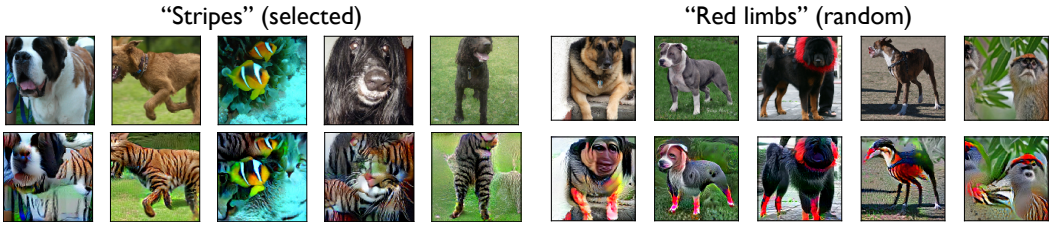

Figure 11: Visualization of the results from maximizing a chosen (left) and a *random* (right) representation coordinate starting from *random* images for the Restricted ImageNet dataset. In each figure, the top row has the initial images, and the bottom row has a feature added. Additional examples are shown in Appendix B.4.1.

results in the corresponding feature being introduced in a continuous manner. It is hence possible to stop this process relatively early to ensure that the content of the original image is preserved. As a heuristic, we stop the optimization process as soon as the desired feature attains a larger value than all the other coordinates of the representation. We visualize the result of this process for a variety of input images and activation coordinates in Figure 11, where *"stripes"* and *"red limbs"* are introduced seamlessly into images without any processing or regularization [2].

5 Related Work

Inverting representations. Previous methods for inverting learned representations typically either solve an optimization problem similar to (1) while imposing a "natural image" prior on the input Mahendran & Vedaldi (2015); Yosinski et al. (2015); Ulyanov et al. (2017) or train a separate model to perform the inversion Kingma & Welling (2015); Dosovitskiy & Brox (2016b;a). Note that since these methods introduce priors or additional components into the inversion process, their results are not fully faithful to the model. In an orthogonal direction, it is possible to construct models that are analytically invertible by construction Dinh et al. (2014; 2017); Jacobsen et al. (2018); Behrmann et al. (2018). However, the representations learned by these models do not seem to be perceptually meaningful (for instance, interpolating between points in the representation space does not lead to perceptual input space interpolations Jacobsen et al. (2018)). Another notable distinction between the inversions shown here and invertible networks is that the latter are an exactly invertible map from $\mathbb{R}^d \to \mathbb{R}^d$, while the former shows that we can approximately recover the original input in $\mathbb{R}^d$ from a representation in $\mathbb{R}^k$ for $k \ll d$.

Feature visualization. Typical methods for visualizing features or classes learned by deep networks follow an optimization-based approach, optimizing objectives similar to objective (5). Since this optimization does not lead to meaningful visualizations directly, these methods incorporate domain-specific input priors (either hand-crafted Nguyen et al. (2015) or learned Nguyen et al. (2016; 2017)) and regularizers Simonyan et al. (2013); Mordvintsev et al. (2015); Oygard (2015);

[2] We repeat this process with many additional random images and random features in Appendix B.4.1.

Yosinski et al. (2015); Tyka (2016); Olah et al. (2017) to produce human-discernible visualizations. The key difference of our work is that we avoid the use of such priors or regularizers altogether, hence producing visualizations that are fully based on the model itself without introducing any additional bias.

Semantic feature manipulation. The latent space of generative adversarial networks (GANs) Goodfellow et al. (2014) tends to allow for "semantic feature arithmetic" Radford et al. (2016); Larsen et al. (2016) (similar to that in word2vec embeddings Mikolov et al. (2013)) where one can manipulate salient input features using latent space manipulations. In a similar vein, one can utilize an image-to-image translation framework to perform such manipulation (e.g. transforming horses to zebras), although this requires a task-specific dataset and model Zhu et al. (2017). Somewhat orthogonally, it is possible to utilize the deep representations of *standard* models to perform semantic feature manipulations; however such methods tend to either only perform well on datasets where the inputs are center-aligned Upchurch et al. (2017), or are restricted to a small set of manipulations Gatys et al. (2016).

6 Conclusion

We show that the learned representations of robustly trained models align much more closely with our idealized view of neural network embeddings as extractors of human-meaningful, high-level features. After highlighting certain shortcomings of standard deep networks and their representations, we demonstrate that robust optimization can actually be viewed as inducing a *human prior* over the features that models are able to learn. In this way, one can view the *robust representations* that result from this prior as feature extractors that are more aligned with human perception.

In support of this view, we demonstrate that robust representations overcome the challenges identified for standard representations: they are approximately invertible, and moving towards an image in representation space seems to entail recovering salient features of that image in pixel space. Furthermore, we show that robust representations can be directly visualized with first-order methods without the need for post-processing or regularization, and also yield much more human-understandable features than standard models (even when they are visualized with regularization). These two properties (inversion and direct feature visualization), in addition to serving as illustrations of the benefits of robust representations, also enable direct modes of input manipulation (interpolation and feature manipulation, respectively).

Overall, our findings highlight robust optimization as a framework to enforce feature priors on learned models. We believe that further exploring this paradigm will lead to models that are significantly more human-aligned while enabling a wide range of new modes of interactions.

REFERENCES

Julius Adebayo, Justin Gilmer, Michael Muelly, Ian Goodfellow, Moritz Hardt, and Been Kim. Sanity checks for saliency maps. In *Neural Information Processing Systems (NeurIPS)*, 2018.

Anish Athalye, Nicholas Carlini, and David A. Wagner. Obfuscated gradients give a false sense of security: Circumventing defenses to adversarial examples. In *International Conference on Machine Learning (ICML)*, 2018.

David Bau, Jun-Yan Zhu, Jonas Wulff, William Peebles, Hendrik Strobelt, Bolei Zhou, and Antonio Torralba. Inverting layers of a large generator. In *ICLR Debugging Machine Learning Models Workshop*, 2019.

Jens Behrmann, Will Grathwohl, Ricky T. Q. Chen, David Duvenaud, and Jörn-Henrik Jacobsen. Invertible residual networks. In *arXiv preprint arXiv:1811.00995*, 2018.

Y. Bengio, A. Courville, and P. Vincent. Representation learning: A review and new perspectives. 2013.

Yoshua Bengio. Talk abstract: Learning high-level representations for agents, 2019. URL https://calendar.mit.edu/event/yoshua_bengio_learning_high-level_representations_for_agents#.XYozli2ZNhF. Abstract for talk given at MIT.

Battista Biggio and Fabio Roli. Wild patterns: Ten years after the rise of adversarial machine learning. 2018.

Wieland Brendel and Matthias Bethge. Approximating CNNs with bag-of-local-features models works surprisingly well on imagenet. In *International Conference on Learning Representations (ICLR)*, 2019.

Andrew Brock, Jeff Donahue, and Karen Simonyan. Large scale GAN training for high fidelity natural image synthesis. In *International Conference on Learning Representations (ICLR)*, 2019.

Ronan Collobert and Jason Weston. A unified architecture for natural language processing: Deep neural networks with multitask learning. In *Proceedings of the 25th international conference on Machine learning*, pp. 160–167, 2008.

John M. Danskin. *The Theory of Max-Min and its Application to Weapons Allocation Problems*. 1967.

Laurent Dinh, David Krueger, and Yoshua Bengio. Nice: Non-linear independent components estimation. In *arXiv preprint arXiv:1410.8516*, 2014.

Laurent Dinh, Jascha Sohl-Dickstein, and Samy Bengio. Density estimation using real nvp. In *International Conference on Learning Representations (ICLR)*, 2017.

Jeff Donahue, Yangqing Jia, Oriol Vinyals, Judy Hoffman, Ning Zhang, Eric Tzeng, and Trevor Darrell. Decaf: A deep convolutional activation feature for generic visual recognition. In *International conference on machine learning (ICML)*, 2014.

Alexey Dosovitskiy and Thomas Brox. Generating images with perceptual similarity metrics based on deep networks. In *neural information processing systems (NeurIPS)*, 2016a.

Alexey Dosovitskiy and Thomas Brox. Inverting visual representations with convolutional networks. In *Computer Vision and Pattern Recognition (CVPR)*, 2016b.

Kunihiko Fukushima. Neocognitron: A self-organizing neural network model for a mechanism of pattern recognition unaffected by shift in position. *Biological cybernetics*, 1980.

Leon A Gatys, Alexander S Ecker, and Matthias Bethge. Image style transfer using convolutional neural networks. In *computer vision and pattern recognition (CVPR)*, 2016.

Robert Geirhos, Patricia Rubisch, Claudio Michaelis, Matthias Bethge, Felix A. Wichmann, and Wieland Brendel. Imagenet-trained CNNs are biased towards texture; increasing shape bias improves accuracy and robustness. In *International Conference on Learning Representations*, 2019.

Ross Girshick, Jeff Donahue, Trevor Darrell, and Jitendra Malik. Rich feature hierarchies for accurate object detection and semantic segmentation. In *computer vision and pattern recognition (CVPR)*, pp. 580–587, 2014.

Ian Goodfellow, Jean Pouget-Abadie, Mehdi Mirza, Bing Xu, David Warde-Farley, Sherjil Ozair, Aaron Courville, and Yoshua Bengio. Generative adversarial nets. In *neural information processing systems (NeurIPS)*, 2014.

Ian Goodfellow, Yoshua Bengio, and Aaron Courville. *Deep Learning*. MIT Press, 2016.

Ian J Goodfellow, Jonathon Shlens, and Christian Szegedy. Explaining and harnessing adversarial examples. In *International Conference on Learning Representations (ICLR)*, 2015.

Kaiming He, Xiangyu Zhang, Shaoqing Ren, and Jian Sun. Delving deep into rectifiers: Surpassing human-level performance on imagenet classification. In *international conference on computer vision (ICCV)*, 2015.

Kaiming He, Xiangyu Zhang, Shaoqing Ren, and Jian Sun. Deep residual learning for image recognition. In *Conference on Computer Vision and Pattern Recognition (CVPR)*, 2016.

Andrew Ilyas, Shibani Santurkar, Logan Engstrom, Brandon Tran, and Aleksander Madry. Adversarial examples are not bugs, they are features. In *ArXiv preprint arXiv:1905.02175*, 2019.

Jorn-Henrik Jacobsen, Jens Behrmann, Richard Zemel, and Matthias Bethge. Excessive invariance causes adversarial vulnerability. In *International Contemporary on Learning Representations*, 2019.

Jörn-Henrik Jacobsen, Arnold W.M. Smeulders, and Edouard Oyallon. i-revnet: Deep invertible networks. In *International Conference on Learning Representations (ICLR)*, 2018.

Saumya Jetley, Nicholas Lord, and Philip Torr. With friends like these, who needs adversaries? In *Advances in Neural Information Processing Systems (NeurIPS)*, 2018.

Justin Johnson, Alexandre Alahi, and Li Fei-Fei. Perceptual losses for real-time style transfer and super-resolution. In *European conference on computer vision (ECCV)*, 2016.

Diederik P. Kingma and Max Welling. Auto-encoding variational bayes. In *International Conference on Learning Representations (ICLR)*, 2015.

Alex Krizhevsky, Ilya Sutskever, and Geoffrey E Hinton. Imagenet classification with deep convolutional neural networks. In *Advances in Neural Information Processing Systems (NeurIPS)*, 2012.

Anders Boesen Lindbo Larsen, Søren Kaae Sønderby, Hugo Larochelle, and Ole Winther. Autoencoding beyond pixels using a learned similarity metric. In *International Conference on Machine Learning (ICML)*, 2016.

Aleksander Madry, Aleksandar Makelov, Ludwig Schmidt, Dimitris Tsipras, and Adrian Vladu. Towards deep learning models resistant to adversarial attacks. In *International Conference on Learning Representations (ICLR)*, 2018.

Aravindh Mahendran and Andrea Vedaldi. Understanding deep image representations by inverting them. In *computer vision and pattern recognition (CVPR)*, 2015.

Tomas Mikolov, Ilya Sutskever, Kai Chen, Greg S Corrado, and Jeff Dean. Distributed representations of words and phrases and their compositionality. In *Advances in neural information processing systems*, pp. 3111–3119, 2013.

Alexander Mordvintsev, Christopher Olah, and Mike Tyka. Inceptionism: Going deeper into neural networks, 2015. URL `https://ai.googleblog.com/2015/06/inceptionism-going-deeper-into-neural.html`.

Alexander Mordvintsev, Nicola Pezzotti, Ludwig Schubert, and Chris Olah. Differentiable image parameterizations. In *Distill*, 2018.

Anh Nguyen, Jason Yosinski, and Jeff Clune. Deep neural networks are easily fooled: High confidence predictions for unrecognizable images. In *Conference on computer vision and pattern recognition (CVPR)*, 2015.

Anh Nguyen, Alexey Dosovitskiy, Jason Yosinski, Thomas Brox, and Jeff Clune. Synthesizing the preferred inputs for neurons in neural networks via deep generator networks. In *Neural Information Processing Systems (NeurIPS)*, 2016.

Anh Nguyen, Jeff Clune, Yoshua Bengio, Alexey Dosovitskiy, and Jason Yosinski. Plug & play generative networks: Conditional iterative generation of images in latent space. In *Conference on Computer Vision and Pattern Recognition (CVPR)*, 2017.

Chris Olah, Alexander Mordvintsev, and Ludwig Schubert. Feature visualization. In *Distill*, 2017.

Audun Oygard. Visualizing googlenet classes, 2015. URL `https://www.auduno.com/2015/07/29/visualizing-googlenet-classes/`.

Alec Radford, Luke Metz, and Soumith Chintala. Unsupervised representation learning with deep convolutional generative adversarial networks. In *International Conference on Learning Representations (ICLR)*, 2016.

Olga Russakovsky, Jia Deng, Hao Su, Jonathan Krause, Sanjeev Satheesh, Sean Ma, Zhiheng Huang, Andrej Karpathy, Aditya Khosla, Michael Bernstein, Alexander C. Berg, and Li Fei-Fei. ImageNet Large Scale Visual Recognition Challenge. In *International Journal of Computer Vision (IJCV)*, 2015.

Karen Simonyan and Andrew Zisserman. Very deep convolutional networks for large-scale image recognition. In *International Conference on Learning Representations (ICLR)*, 2015.

Karen Simonyan, Andrea Vedaldi, and Andrew Zisserman. Deep inside convolutional networks: Visualising image classification models and saliency maps. *arXiv preprint arXiv:1312.6034*, 2013.

Dong Su, Huan Zhang, Hongge Chen, Jinfeng Yi, Pin-Yu Chen, and Yupeng Gao. Is robustness the cost of accuracy? a comprehensive study on the robustness of 18 deep image classification models. In *European Conference on Computer Vision (ECCV)*, 2018.

Christian Szegedy, Wojciech Zaremba, Ilya Sutskever, Joan Bruna, Dumitru Erhan, Ian Goodfellow, and Rob Fergus. Intriguing properties of neural networks. In *International Conference on Learning Representations (ICLR)*, 2014.

Dimitris Tsipras, Shibani Santurkar, Logan Engstrom, Alexander Turner, and Aleksander Madry. Robustness may be at odds with accuracy. In *International Conference on Learning Representations (ICLR)*, 2019.

Mike Tyka. Class visualization with bilateral filters, 2016. URL `https://mtyka.github.io/deepdream/2016/02/05/bilateral-class-vis.html`.

Dmitry Ulyanov, Andrea Vedaldi, and Victor Lempitsky. Deep image prior. In *ArXiv preprint arXiv:1711.10925*, 2017.

Paul Upchurch, Jacob Gardner, Geoff Pleiss, Robert Pless, Noah Snavely, Kavita Bala, and Kilian Weinberger. Deep feature interpolation for image content changes. In *conference on computer vision and pattern recognition (CVPR)*, 2017.

Abraham Wald. Statistical decision functions which minimize the maximum risk. In *Annals of Mathematics*, 1945.

Jason Yosinski, Jeff Clune, Anh Nguyen, Thomas Fuchs, and Hod Lipson. Understanding neural networks through deep visualization. In *arXiv preprint arXiv:1506.06579*, 2015.

Richard Zhang, Phillip Isola, Alexei A Efros, Eli Shechtman, and Oliver Wang. The unreasonable effectiveness of deep features as a perceptual metric. In *Computer Vision and Pattern Recognition (CVPR)*, 2018.

Tianyuan Zhang and Zhanxing Zhu. Interpreting adversarially trained convolutional neural networks. In *International Conference on Machine Learning (ICML)*, 2019.

Jun-Yan Zhu, Taesung Park, Phillip Isola, and Alexei A Efros. Unpaired image-to-image translation using cycle-consistent adversarial networks. In *international conference on computer vision(ICCV)*, 2017.

A EXPERIMENTAL SETUP

A.1 DATASETS

In the main text, we perform all our experimental analysis on the Restricted ImageNet dataset Tsipras et al. (2019) which is obtained by grouping together semantically similar classes from ImageNet into 9 super-classes shown in Table 1. Attaining robust models for the complete ImageNet dataset is known to be challenging, both due to the hardness of the learning problem itself, as well as the computational complexity.

For the sake of completeness, we also replicate our experiments feature visualization and representation inversion on the complete ImageNet dataset Russakovsky et al. (2015) in Appendices B.1.4 and B.2.4—in particular, cf. Figures 16 and 20.

Table 1: Classes used in the Restricted ImageNet model. The class ranges are inclusive.

Class	**Corresponding ImageNet Classes**
"Dog"	151 to 268
"Cat"	281 to 285
"Frog"	30 to 32
"Turtle"	33 to 37
"Bird"	80 to 100
"Primate"	365 to 382
"Fish"	389 to 397
"Crab"	118 to 121
"Insect"	300 to 319

A.2 MODELS

We use the ResNet-50 architecture He et al. (2016) for our adversarially trained classifiers on all datasets. Unless otherwise specified, we use standard ResNet-50 classifiers trained using empirical risk minimization as a baseline in our experiments. Additionally, it has been noted in prior work that among standard classifiers, VGG networks Simonyan & Zisserman (2015) tend to have better-behaved representations and feature visualizations Mordvintsev et al. (2018). Thus, we also compare against standard VGG16 networks in the subsequent appendices. All models are trained with data augmentation, momentum 0.9 and weight decay $5e^{-4}$. Other hyperparameters are provided in Tables 2 and 3.

The exact procedure used to train robust models along with the corresponding hyperparameters are described in Section A.3. For standard (not adversarially trained) classifiers on the complete 1k-class ImageNet dataset, we use pre-trained models provided in the PyTorch repository[3].

Table 2: Standard hyperparameters for the models trained in the main paper.

Dataset	Model	Arch.	Epochs	LR	Batch Size	LR Schedule
Restricted ImageNet	standard	ResNet-50	110	0.1	256	Drop by 10 at epochs $\in [30, 60]$
Restricted ImageNet	robust	ResNet-50	110	0.1	256	Drop by 10 at epochs $\in [30, 60]$
ImageNet	robust	ResNet-50	110	0.1	256	Drop by 10 at epochs $\in [100]$

Test performance of all the classifiers can be found in Section A.4. Specific parameters used to study the properties of learned representations are described in Section A.6.

[3] https://pytorch.org/docs/stable/torchvision/models.html

A.3 ADVERSARIAL TRAINING

To obtain robust classifiers, we employ the adversarial training methodology proposed in Madry et al. (2018). Specifically, we train against a projected gradient descent (PGD) adversary, starting from a random initial perturbation of the training data. We consider adversarial perturbations in ℓ_2 norm. Unless otherwise specified, we use the values of ϵ provided in Table 3 to train/evaluate our models (the images themselves lie in the range $[0, 1]$).

Table 3: Hyperparameters used for adversarial training.

Dataset	ϵ	# steps	Step size
Restricted ImageNet	3.0	7	0.5
ImageNet	3.0	7	0.5

A.4 MODEL PERFORMANCE

Standard test performance for the models used in the paper are presented in Table 4 for the Restricted ImageNet dataset and in Table 5 for the complete ImageNet dataset.

Additionally, we report adversarial accuracy of both standard and robust models. Here, adversarial accuracies are computed against a PGD adversary with 20 steps and step size of 0.375. (We also evaluated against a stronger adversary using more steps (100) of PGD, however this had a marginal effect on the adversarial accuracy of the models.)

Table 4: Test accuracy for standard and robust models on the Restricted ImageNet dataset.

Model	Standard	Adversarial (eps=3.0)
Standard VGG16	98.22%	2.17%
Standard ResNet-50	98.01%	4.74%
Robust ResNet-50	92.39%	81.91%

Table 5: Top-1 accuracy for standard and robust models on the ImageNet dataset.

Model	Standard	Adversarial (eps=3.0)
Standard VGG16	73.36%	0.35%
Standard ResNet-50	76.13%	0.13%
Robust ResNet-50	57.90%	35.16%

A.5 IMAGE INTERPOLATIONS

A natural consequence of the "natural invertibility" property of robust representations is the ability to synthesize natural interpolations between any two inputs $x_1, x_2 \in \mathbb{R}^n$. In particular, given two images x_1 and x_2, we define the λ-*interpolate* between them as

$$x_\lambda = \min_x \| (\lambda \cdot R(x_1) + (1 - \lambda) \cdot R(x_2)) - R(x) \|_2. \tag{6}$$

where, for a given λ, we find x_λ by solving (6) with projected gradient descent. Intuitively, this corresponds to linearly interpolating between the points in representation space and then finding a point in image space that has a similar representation. To construct a length-$(T + 1)$ interpolation, we choose $\lambda = \{0, \frac{1}{T}, \frac{2}{T}, \dots 1\}$. The resulting interpolations, shown in Figure 12, demonstrate that the λ-interpolates of robust representations correspond to a meaningful feature interpolation between images. (For standard models constructing meaningful interpolations is impossible due to the brittleness identified in Section 2—see Appendix B.2.3 for details.)

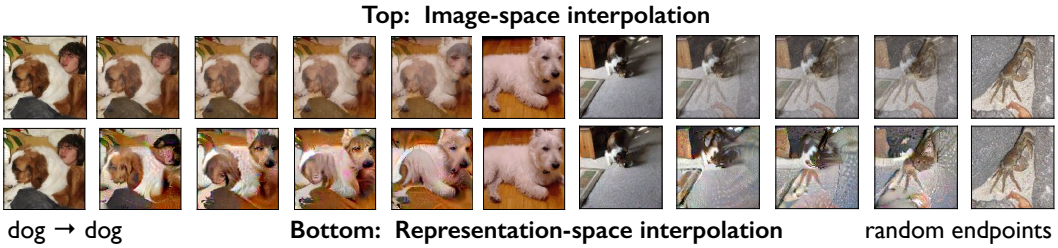

Figure 12: Image interpolation using robust representations compared to their image-space counterparts. The former appear perceptually plausible while the latter exhibit ghosting artifacts. For pairs of images from the Restricted ImageNet test set, we solve (6) for λ varying between zero and one, i.e., we match linear interpolates in representation space. Additional interpolations appear in Appendix B.3.1 Figure 21. We demonstrate the ineffectiveness of interpolation with standard representations in Appendix B.3.2 Figure 22.

Relation to other interpolation methods. We emphasize that linearly interpolating in robust representation space works for *any* two images. This generality is in contrast to interpolations induced by GANs (e.g. (Radford et al., 2016; Brock et al., 2019)), which can only interpolate between images generated by the generator. (Reconstructions of out-of-range images tend to be decipherable but rather different from the originals Bau et al. (2019).) It is worth noting that even for models with analytically invertible representations, interpolating in representation space does not yield semantic interpolations Jacobsen et al. (2018).

A.6 Parameters used in studies of robust/standard representations

A.6.1 Finding representation-feature correspondence

Dataset	ϵ	# steps	Step size
Restricted ImageNet/ImageNet	1000	200	1

A.6.2 Inverting representations and interpolations

Dataset	ϵ	# steps	Step size
Restricted ImageNet/ImageNet	1000	10000	1

B OMITTED FIGURES

B.1 DO LEARNED REPRESENTATIONS CAPTURE MEANINGFUL FEATURES?

B.1.1 FEATURES LEARNED BY A RANDOM SUBSET OF ROBUST REPRESENTATIONS

Figure 13: Correspondence between image-level features and representations learned by a robust model on the Restricted ImageNet dataset. Starting from randomly chosen seed inputs (noise/images), we use a constrained optimization process to identify input features that maximally activate a given component of the representation vector (cf. Appendix A.6.1 for details). Specifically, (*left column*): inputs to the optimization process, and (*subsequent columns*): features that activate randomly chosen representation components, along with the predicted class of the feature.

B.1.2 FEATURES LEARNED BY SELECT ROBUST REPRESENTATIONS

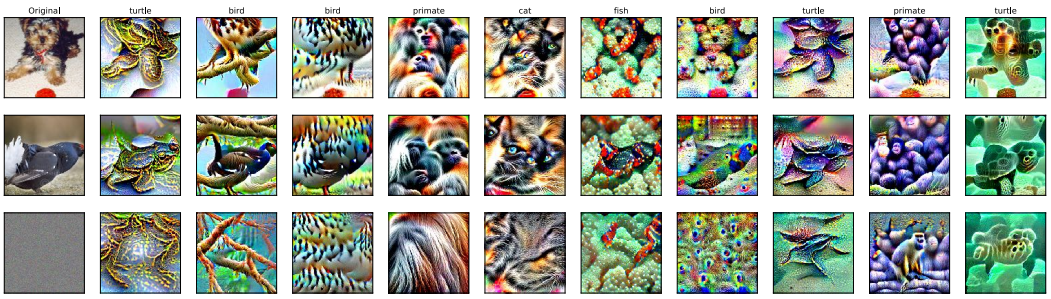

Figure 14: Correspondence between image-level features and representations learned by a robust model on the Restricted ImageNet dataset. Starting from randomly chosen seed inputs (noise/images), we use a constrained optimization process to identify input features that maximally activate a given component of the representation vector (cf. Appendix A.6.1 for details). Specifically, (*left column*): inputs to the optimization process, and (*subsequent columns*): features that activate select representation components, along with the predicted class of the feature.

B.1.3 ADDITIONAL COMPARISON OF FEATURES LEARNED BY STANDARD AND ROBUST CLASSIFIERS

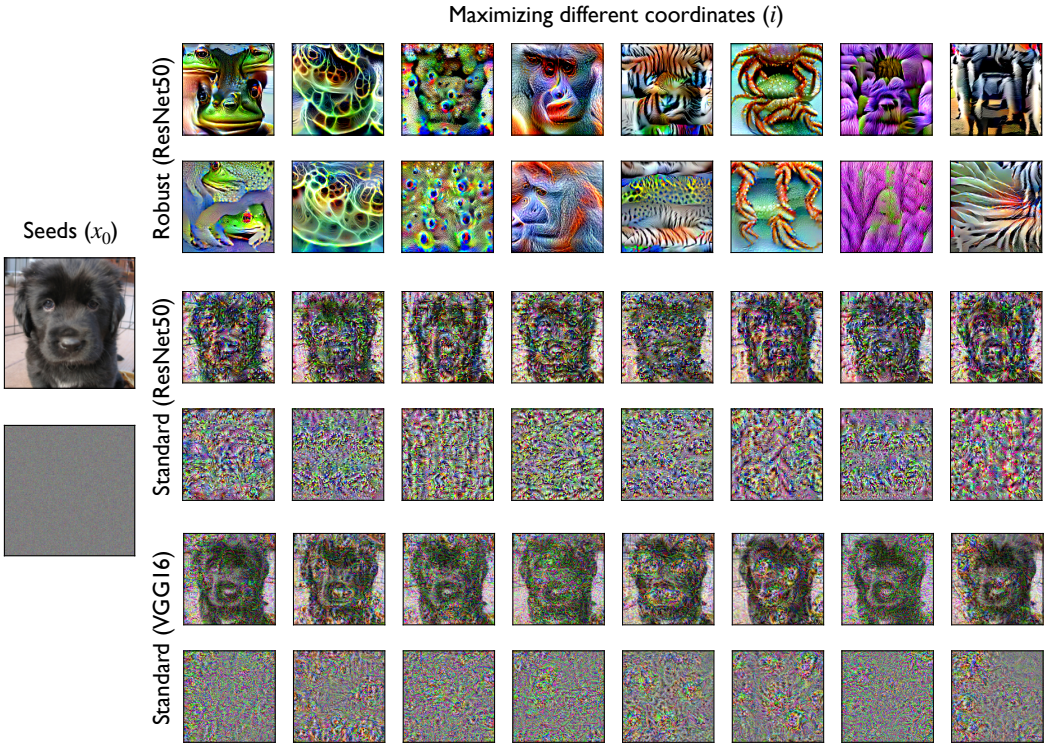

Figure 15: Correspondence between image-level patterns and activations learned by standard and robust models on the Restricted ImageNet dataset. Starting from randomly chosen seed inputs (noise/images), we use PGD to find inputs that (locally) maximally activate a given component of the representation vector (cf. Appendix A.6.1 for details). In the left column we have the original inputs (selected *randomly*), and in subsequent columns we visualize the result of the optimization (5) for different activations, with each row starting from the same (far left) input for (*top*): a robust (adversarially trained) ResNet-50 model, (*middle*): a standard ResNet-50 model and (*bottom*): a standard VGG16 model.

B.1.4 FEATURES LEARNED BY STANDARD AND ROBUST CLASSIFIERS FOR THE IMAGENET DATASET

Figure 16: Correspondence between image-level patterns and activations learned by standard and robust models on the complete ImageNet dataset. Starting from randomly chosen seed inputs (noise/images), we use PGD to find inputs that (locally) maximally activate a given component of the representation vector (cf. Appendix A.6.1 for details). In the left column we have the original inputs (selected *randomly*), and in subsequent columns we visualize the result of the optimization (5) for different activations, with each row starting from the same (far left) input for (*top*): a robust (adversarially trained) ResNet-50 model, (*middle*): a standard ResNet-50 model and (*bottom*): a standard VGG16 model.

B.2 INVERTIBILITY OF ROBUST REPRESENTATIONS

B.2.1 RECONSTRUCTION OF TEST SET IMAGES

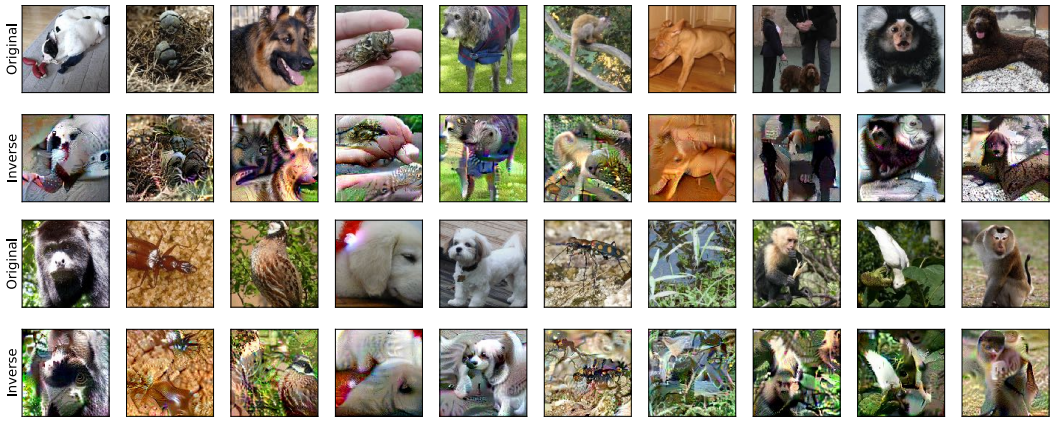

(a)

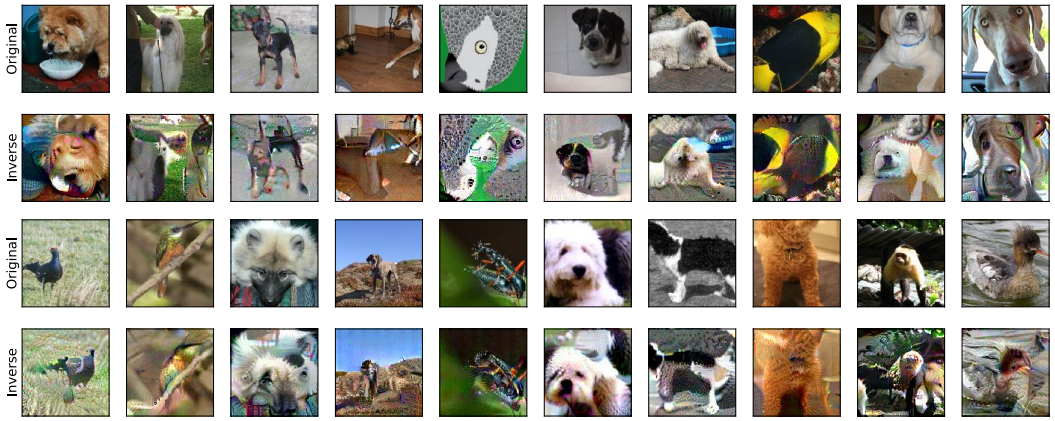

(b)

Figure 17: Robust representations yield semantically meaningful inverses: *Original*: randomly chosen test set images from the Restricted ImageNet dataset; *Inverse*: images obtained by inverting the representation of the corresponding image in the top row by solving the optimization problem (1) starting from: (a) different test images and (b) Gaussian noise.

B.2.2 RECONSTRUCTION OF OUT-OF-DISTRIBUTION INPUTS

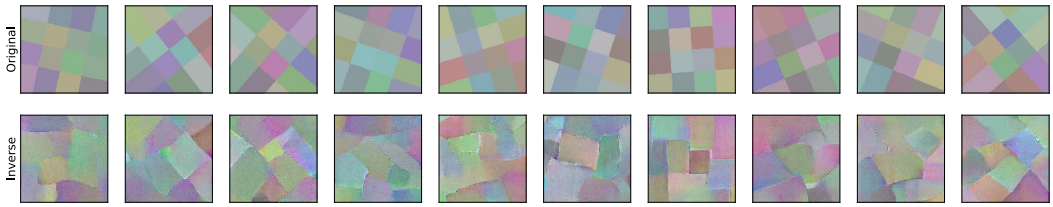

(a) Random kaleidoscope patterns.

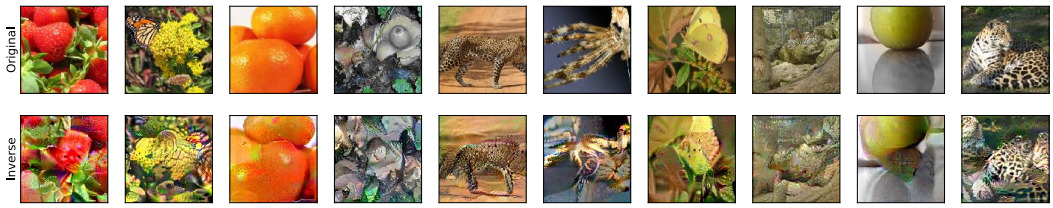

(b) Samples from other ImageNet classes outside what the model is trained on.

Figure 18: Robust representations yield semantically meaningful inverses: (*Original*): randomly chosen out-of-distribution inputs; (*Inverse*): images obtained by inverting the representation of the corresponding image in the top row by solving the optimization problem (1) starting from Gaussian noise.

B.2.3 INVERTIBILITY OF STANDARD REPRESENTATIONS

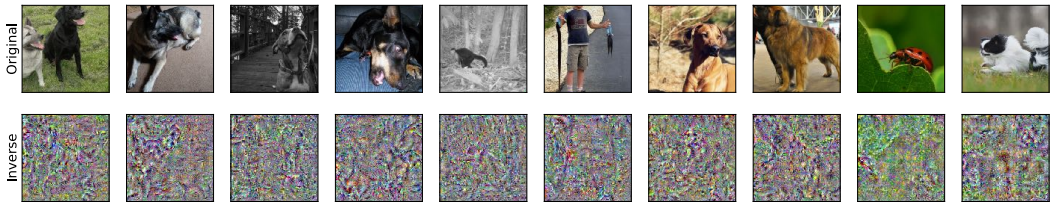

Figure 19: Standard representations *do not* yield semantically meaningful inverses: (*Original*): randomly chosen test set images from the Restricted ImageNet dataset; (*Inverse*): images obtained by inverting the representation of the corresponding image in the top row by solving the optimization problem (1) starting from Gaussian noise.

B.2.4 INVERTIBILITY OF REPRESENTATIONS FOR THE IMAGENET DATASET

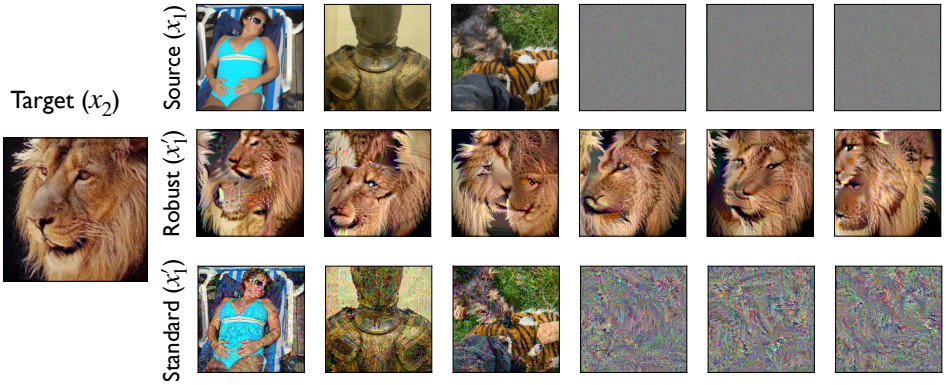

Figure 20: Visualization of inputs that are mapped to similar representations by models trained on the ImageNet dataset. *Target* (x_2) & *Source* (x_1): random examples image from the test set; *Robust* and *Standard* (x_1'): result of minimizing the objective (4) to match (in ℓ_2-distance) the representation of the target image starting from the corresponding source image for (*top*): a robust (adversarially trained) and (*bottom*): a standard model respectively. For the robust model, we observe that the resulting images are perceptually similar to the target image in terms of high-level features, while for the standard model they often look more similar to the source image which is the seed for the optimization process.

B.3 IMAGE INTERPOLATIONS

B.3.1 ADDITIONAL INTERPOLATIONS FOR ROBUST MODELS

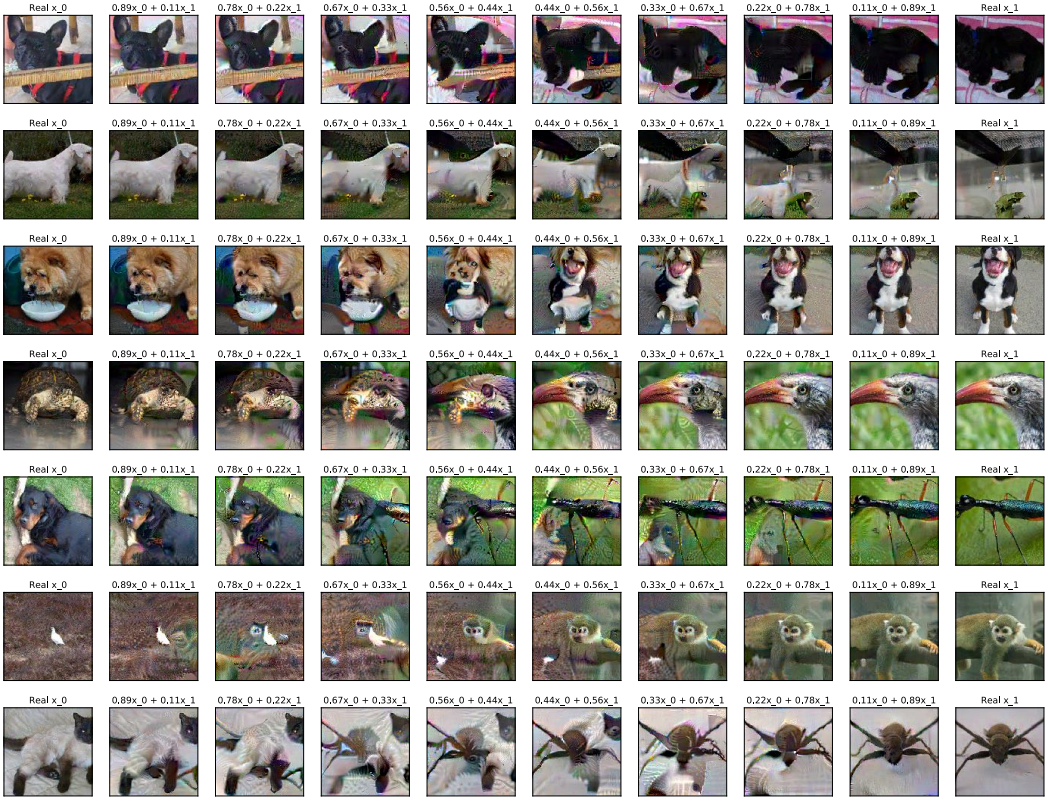

Figure 21: Additional image interpolation using robust representations. To find the interpolation in input space, we construct images that map to linear interpolations of the endpoints in robust representation space. Concretely, for randomly selected pairs from the Restricted ImageNet test set, we use (1) to find images that match to the linear interpolates in representation space (6).

B.3.2 STANDARD MODELS YIELD SUPERIMPOSED-LIKE INTERPOLATIONS

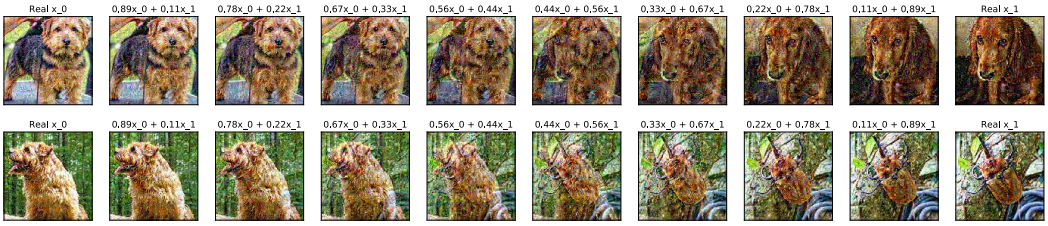

Figure 22: Image interpolation using standard representations. To find the interpolation in input space, we construct images that map to linear interpolations of the endpoints in standard representation space. Concretely, for randomly selected pairs from the Restricted ImageNet test set, we use (1) to find images that match to the linear interpolates in representation space (6). Image space interpolations from the standard model appear to be significantly less meaningful than their robust counterparts. They are visibly similar to linear interpolation directly in the input space, which is in fact used to seed the optimization process.

B.4 EXPLORATION VIA ADDING FEATURES

B.4.1 ADDITIONAL EXAMPLES OF FEATURE ADDITION

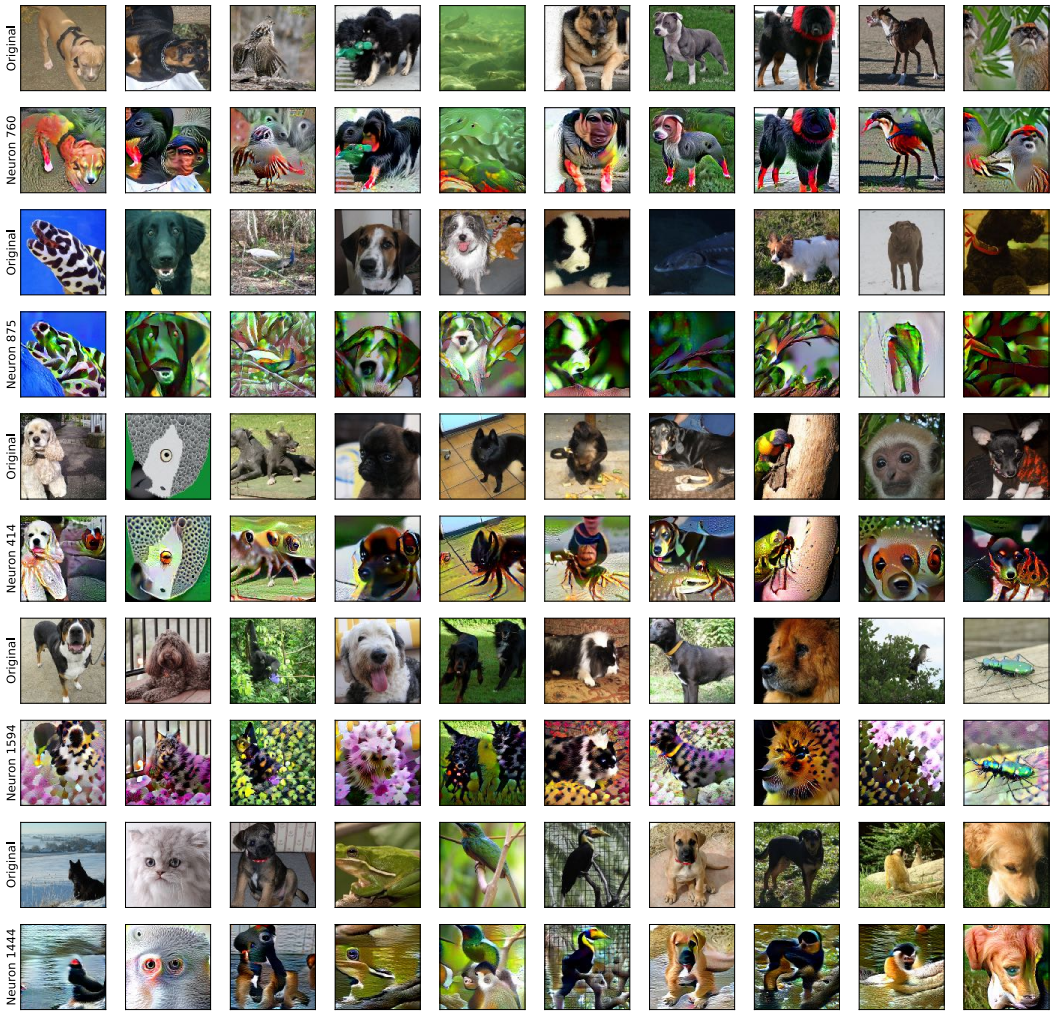

Figure 23: Visualization of the results adding various neurons, labelled on the left, to randomly chosen test images. The rows alternate between the original test images, and those same images with an additional feature arising from maximizing the corresponding neuron.